# Nutrient competition as a determinant for cancer growth

M. Scalerandi,[1] A. Romano,[1] G. P. Pescarmona,[2] P. P. Delsanto,[1] and C. A. Condat[3]
[1]*INFM, Dipartimento di Fisica, Politecnico di Torino, Torino, Italy*
[2]*Dipartimento di Genetica, Biologia e Chimica Medica, Università di Torino, Torino, Italy*
[3]*Universidad Nacional de Córdoba, Córdoba, Argentina*
(Received 19 March 1998; revised manuscript received 28 July 1998)

Competition for available nutrients is known to be crucial for cancer development. Based on this fact, a model is proposed that can describe the manifold of morphologies and growth rates characteristic of tumoral growth. The formulation of a consistent set of rules governing the microscopic interactions leads to a system of coupled nonlinear iteration equations. These equations contain both deterministic and stochastic terms and are amenable to direct numerical simulation. They allow us to test the effects of such parameters as the availability, diffusivity, and binding rate of nutrients and the mobility, death, and multiplication rates of cancer cells on tumor morphology and development. Detailed numerical solutions are presented.
[S1063-651X(99)03402-9]

PACS number(s): 87.10.+e, 02.60.Cb

## I. INTRODUCTION

The understanding of the dynamics of tumoral growth is one of the great challenges of modern science. The interest of the problem has led to the formulation of numerous growth models. On the experimental side, new techniques are continuously enriching our knowledge of the phenomenology of this growth and, consequently, imposing additional constraints on the models being developed. An excellent survey of the state of the art in tumor modeling can be found in a recent book edited by Adam and Bellomo [1]. The initial stages of tumor evolution have been described using the deterministic diffusion-controlled growth of spheroids. One of the first steps in this direction was Burton's model [2]. Burton considered a spherically symmetric tumor growing under conditions of diffusive equilibrium, and was able to obtain formulas for the radii of the tumor and its necrotic core.

A few years later, Glass introduced a growth inhibitor in a model of one-dimensional growth, showing how it could lead to a bounded tumor [3]. An extension of this model to three dimensions was due to Shymko and Glass [4]. These authors found that, depending on the choice of parameters, it was possible to obtain both limited and unlimited spheroidal growth. The effect of nonsymmetric perturbations was investigated by Greenspan [5]. More recently [6], Chaplain and co-workers addressed the issue of nonlinear diffusion, showing that it leads to results similar to those obtained by assuming the existence of a nonlinear source term. One of the most sophisticated mathematical descriptions of the various stages of cancer growth, including angiogenesis and the vascular stage, is that presented by Chaplain [7].

In this paper we propose a model whose philosophy is completely different from that of previous mathematical models. Rather than trying to obtain analytical solutions that mimic the kinetics of cell population growth, we pay close attention to the local evolution and to the role of a set of relevant parameters characterizing cell proliferation. A computer simulation is used to generate specific predictions. This procedure allows us to model, without any parameter fitting, some of the crucial events taking place at the cellular level. It is also capable of taking into account fluctuations and irregularities in the nutrient distributions and in the cell populations. It seems clear to us that, except in its very early stages, or in a very homogenous and controlled environment, a growing tumor will seldom preserve a shape that can be adequately described by any manageably simple set of analytical functions.

Nutrients introduced with the diet are carried through the vascular system by the blood, cross the vessel walls, and diffuse through the tissue towards the individual cells. Essential nutrients for eukaryotic cells include some amino acids, glucose, and transition metals such as iron, zinc, and copper. Oxygen is a limiting factor for many cellular functions, including differentiation, respiration, and mechanical work, but it does not significantly restrict cell proliferation, which is supported by anaerobic glycolysis and does not involve enzymatic steps requiring oxygen [8]. When the amount of an essential nutrient is limited within a specific environment, the growth rate of a given cell population is controlled by its ability to compete for it. We will show how the manifold of cancer morphologies emerges from a model that properly accounts for the competition for nutrients among the various cell populations.

The high proliferation rate of cancer cells makes them especially vulnerable to nutrient deprivation. For this reason, behind a rapidly evolving tumoral front, a necrotic core, composed mostly of dead cells, usually develops. As a consequence, we need to consider at least three different cell populations coexisting in the tumor-affected tissue: healthy cells, cancer cells, and dead cells.

Although the model is formulated taking into account the presence of many nutrients, solutions are obtained by assuming that crucial processes are controlled by a single critical nutrient. There are reasons to believe that iron can often play this role. In fact, beyond its well-known role in oxygen transport in many redox reactions, including mitochondrial electron transport, in all the hydroxylase reactions, and in the

 

synthesis of uric acid, it is used, in the form of an iron-sulfur complex, in the synthesis of deoxyribonucleotides from ribonucleotides. Since deoxyribonucleotides are essential for DNA synthesis and, therefore, for reproduction, iron is a requisite nutrient for the reproduction of all living organisms [9]. Indeed, it is known that a cancer cell, like any other cell, reproduces when enough iron is available; furthermore, cells treated with iron chelators detach and die [10], the intermediate reaction to a sharp iron deficiency being detachment and diffusion [11]. On the other hand, the organs where metastatic cancer cells more often come to a stop are those, like bone marrow, liver, and lung, whose iron concentration is highest.

Iron uptake is mediated by siderophores, special carriers whose synthesis is regulated by the actual cellular need of iron. On the basis of the pattern and amount of siderophores produced by the cells [12] and of the number of corresponding receptors, it is possible to forecast the growth of the cell population under study, by assuming that the iron availability in the selected environment and the ability of the competing populations to produce siderophores and receptors are known [13].

Since the complexity of the problem requires that for all nontrivial cases we obtain our solutions numerically, we write the equations defining our model directly in their discretized forms. For simplicity, all of our examples are worked out in two dimensions. This restriction on the dimensionality is not really important, since the manifold of evolution patterns arising in two dimensions seems vast enough to capture all the important features of a general description of cancer growth. If the geometry of a given problem required an explicit three-dimensional solution, our formalism could be extended without difficulties.

The problems of cancer growth, and, more generally, of cell motion and cell pattern formation, have been largely ignored in the physics literature. Perhaps this situation is starting to change [14–17]. Two papers, one theoretical and the other experimental, containing elements closely related to some of the ingredients used in our model, have appeared very recently. Schweitzer, Ebeling, and Tilch have investigated the motion of Brownian particles that have the ability of storing energy in an internal depot, transporting it along, and transforming it into kinetic energy [16] (in our model cancer cells transport the bound nutrient along). Halvorsrud and Wagner have performed a careful study of the growth of the plasmodium stage of the slime mold Physarum on a substrate containing a nonuniform nutrient distribution [17]. The plasmodial behavior was found to comprise a feeding phase characterized by nutrient absorption and plasmodium growth, and a searching phase characterized by the migration of the plasmodial front in a non-nutrient area.

In the next section we present our model, assuming that several nutrients are simultaneously relevant for tumor evolution. A detailed numerical study of the model solutions is given in Sec. III, where we will consider a single crucial nutrient and determine the importance of various environmental parameters. Finally, in Sec. IV we conclude by suggesting some possibilities for future work.

## II. MODEL

In this section we develop our model. We start by describing nutrient absorption and transport in healthy tissues, where we later introduce a cancer seed. We then state the rules for its evolution and write the set of coupled nonlinear equations that describe the system.

### A. Nutrients in healthy tissue

First, we consider a cancer-free tissue slab, in which $M$ nutrients originate from one or more sources, diffuse, and are consumed by healthy cells. These cells are assumed to be uniformly distributed in the region under consideration. The nutrient concentrations $p_k(\vec{r},t)$ $(k=1,\ldots,M)$ satisfy reaction-diffusion equations. To write these equations, we discretize the diffusion space using a two-dimensional square grid with $(2I+1)\times(2J+1)$ node points. Each node point $(i,j)$ represents a volume element that will generally contain many cells and nutrient molecules.

Let $\alpha_k$, $\gamma_k$, and $S_k(t)$ be, respectively, the diffusion rate for nutrient $k$, its absorption rate by each healthy cell, and its input rate (from external sources). Assuming that the nutrients are noninteracting, we can easily write the equation satisfied by the free nutrient concentration $p_k$ at node point $\vec{i}$:

$$\dot{p}_k(\vec{i},t)=\sum_{i'}^{\mathrm{NN}} \alpha_k[p_k(\vec{i}',t)-p_k(\vec{i},t)]-\gamma_k p_k(\vec{i},t)h+S_k(\vec{i},t). \tag{2.1}$$

Here the first term on the right-hand side corresponds to nutrient diffusion from and to the nearest neighbors of $\vec{i}$, the second term accounts for the free nutrient absorption by a population $h$ of healthy cells, and the last term corresponds to the nutrient sources. In prevascular stages, these sources may be considered as time independent, simply providing a fixed nutrient concentration in some tissue regions.

There are $M$ uncoupled equations for the various nutrients. These equations are valid provided that (i) nutrient diffusion is homogeneous and isotropic and (ii) the absorption of the various nutrients proceeds independently of the presence of other nutrients. The relaxation of assumption (i) would involve the introduction of either local or direction-dependent $\alpha$'s, while the relaxation of assumption (ii) would require the introduction of coupling terms between the equations for the different nutrients.

Equation (2.1) must be complemented by suitable initial and boundary conditions.

### B. Rules for cancer growth

We assume that at time $t=0$ a cancer seed appears at the center of an otherwise completely healthy slab. At later times we will have three coexisting cell populations, which we shall label $h(\vec{i},t)$ (healthy cells), $c(\vec{i},t)$ (cancerous cells), and $d(\vec{i},t)$ (dead cells). The distribution of the cells occupying a given node point will change in time, but we assume that the total node population is conserved:

$$h(\vec{i},t)+c(\vec{i},t)+d(\vec{i},t)=n, \tag{2.2}$$

where $n$ is the total cell population at any node point, assumed to be the same everywhere.

Since the amounts of free and bound nutrients per node determine the triggering of the different growth processes, they must be considered separately: they will be labeled $p_k$ and $q_k$, respectively.

We could formulate the model in such a way that the time evolution of these concentrations and of the cell populations was described by first-order (in time) differential equations. However, since a numerical procedure is, in any case, required to obtain solutions, we will formulate our equations directly in their time-discretized forms.

Next we state the rules that govern the behavior of the cancerous cells, omitting, for brevity, to write explicitly the time dependence, wherever not strictly necessary.

*(1) Feeding.* Free nutrients are transformed into bound nutrients by cancer cell uptake at the rate

$$\tilde{\gamma}_k(\vec{i}) = \tilde{\gamma}_k^{as}\{1-\exp[-\tilde{\Gamma} p_k(\vec{i})/P_N]\}, \tag{2.3}$$

where $\tilde{\Gamma}$ is an iron affinity parameter and $P_N$ a proper normalization factor, and *as* denotes the asymptotic value for $P_k(i)\to\infty$. Equation (2.3) expresses the dependence of the binding rate on the nutrient availability. It must be proportional to the nutrient concentration at low concentrations, while it is likely to saturate at higher concentrations. By a proper choice of units we can impose, for simplicity, $\tilde{\Gamma} = P_N$. An equation similar to Eq. (2.3) should also be written, of course, for healthy cells. Since, however, their iron affinity parameter $\Gamma \ll \tilde{\Gamma}$, a first-order approximation to Eq. (2.3), as included in Eq. (2.1), is sufficient.

*(2) Consumption.* Bound nutrients are consumed by cancer cells at the rate

$$\tilde{\beta}_k(\vec{i}) = \tilde{\beta}_k^{as}\{1-\exp[-q_k(\vec{i})/c(\vec{i})]\}, \tag{2.4}$$

where again a saturation in the consumption rate is assumed. The factor $c(\vec{i})$ has been included in the denominator of the exponent of Eq. (2.4), since a cell can consume only its own bound iron, i.e., on the average, $q_k(\vec{i})/c(\vec{i})$, while it has access to the whole amount $p(\vec{i})$ of free iron.

*(3) Death.* If the average amount of a bound nutrient per cancer cell in a given node $\vec{i}$, $q_k(\vec{i})/c(\vec{i})$, falls below a threshold $Q_{k,D}$, a random number of cancer cells, $r_k(\vec{i}) < c(\vec{i})$, starve and die in the following step. The number of dying cells depends on the importance of the nutrient species, but if the concentration of more than one nutrient has gone at a given time below the corresponding death threshold, the condition $\Sigma r_k(\vec{i}) < c(\vec{i})$ must be satisfied.

*(4) Mitosis.* The availability of sufficiently high quantities of bound nutrients may trigger cancer cell division. If $q_k(\vec{i})/c(\vec{i})$ becomes larger than an upper threshold $Q_{k,M}$ for each nutrient $k$, a properly defined random number of cancerous cells, $r'(\vec{i}) < h(\vec{i})$, replace healthy cells.

*(5) Migration.* If too little of a free nutrient is available, cancerous cells tend to migrate to neighboring nodes looking for a more suitable environment. Of course, the resulting cellular diffusion rate $\tilde{\alpha}_k$ depends on the nutrient species $k$, since the number and efficiency of the sensors put out by the cancer cell to register nutrient abundance in the environment depends on the nutrient species. For simplicity, we assume that only the nutrient $k=1$, which is likely to be iron, is crucial for determining cancer cell migration. Hence we assume that if $p_1(\vec{i})/c(\vec{i}) < P_D$, a random number of cancer cells, $r''(\vec{i}) < c(\vec{i})$, migrate to neighboring nodes. We note that the migrating cancer cells take their bound nutrients along. We also remark that healthy cells must be present at the target node to permit the displacement of the cancer cells. We also assume that $Q_{k,D} < P_D < Q_{k,M}$. Therefore the model allows for a quiescent status of the cancer cells. What happens with the healthy cells when the node in which they are located is invaded by cancer cells? Since they are less mobile and aggressive than cancer cells, and they are generally the weakest element in their competition against them, we assume that they are eliminated when cancerous cells enter the node, in such a way that Eq. (2.2) is preserved.

### C. Equations describing cancer growth

The above stated rules lead to a set of coupled nonlinear equations for the cell populations and nutrient concentrations. At each time step we must first ascertain if one or more of the thresholds defined above have been overcome, and suitably modify the corresponding cell population to account for mitosis or cell death. A suitable algorithm is

$$c(\vec{i},t)\to c(\vec{i},t)\Big\{1-\sum_k r_k(\vec{i})\Theta[Q_{k,D}c(\vec{i})-q_k(\vec{i})] + \prod_k r'(\vec{i})\Theta[q_k(\vec{i})-c(\vec{i})Q_{k,M}]\Big\}. \tag{2.5}$$

Here $\Theta$ is Heaviside's step function. The second and third terms on the right-hand side represent, respectively, the modifications introduced in the cancer cell populations by death and mitosis. The corresponding equation for the dead cell population is

$$d(\vec{i},t)\to d(\vec{i},t)+c(\vec{i},t)\sum_k r_k(\vec{i})\Theta[Q_{k,D}c(\vec{i})-q_k(\vec{i})]. \tag{2.6}$$

The concentration of healthy cells is then recalculated to ensure conservation:

$$h(\vec{i},t) = n - c(\vec{i},t) - d(\vec{i},t). \tag{2.7}$$

After these transformations, we must compute the changes undergone as time advances of one step. The updatings are performed as follows.

(i) Cancer cell population. The population at a node changes because of migration to and from the node. This migration is assumed to be proportional to the population of healthy cells at the target site. Therefore cancer cells move from node $\vec{i}'$ to node $\vec{i}$ at a rate $h(\vec{i})\tilde{\alpha}_1 c(\vec{i}')$, each cell carrying a fraction $q_k(\vec{i}')/c(\vec{i}')$ of bound nutrient $k$. Thus the iteration equation for the cancer cell population is

$$c(\vec{i},t+\tau)=c(\vec{i},t)+\tau\Bigg[h(\vec{i})\sum_{\vec{i}'}^{\mathrm{NN}}\tilde{\alpha}_1(\vec{i}')c(\vec{i}')-\tilde{\alpha}_1(\vec{i})c(\vec{i})\sum_{\vec{i}'}^{\mathrm{NN}}h(\vec{i}')\Bigg], \tag{2.8}$$

where $\tilde{\alpha}_1(\vec{i})=\tilde{\alpha}\Theta[c(i)P_D-p_1(\vec{i})]$, $\tau$ is the time discretization step, and all functions on the right-hand side must be evaluated at the time $t$. Of course, since the migration of a cancer cell depends not only on the local diffusivity but also on the state of the target site, Eq. (2.8) is not the discrete counterpart of a simple diffusion equation.

(ii) Dead cell population. Cells in the necrotic core are static. Thus

$$d(\vec{i},t+\tau)=d(\vec{i},t). \tag{2.9}$$

(iii) Healthy cell population. Again, we use cell number conservation and write

$$h(\vec{i},t+\tau)=n-c(\vec{i},t+\tau)-d(\vec{i},t+\tau). \tag{2.10}$$

(iv) Free nutrient concentration. The equation describing the time evolution of the $k$th free nutrient concentration is

$$p_k(\vec{i},t+\tau)=p_k(\vec{i},t)+\tau\Bigg\{\alpha_k\sum_{\vec{i}'}^{\mathrm{NN}}[p_k(\vec{i}')-p_k(\vec{i})]+S_k(\vec{i})-\gamma_k p_k(\vec{i})h(\vec{i})-\tilde{\gamma}_k(\vec{i})c(\vec{i})\Bigg\}. \tag{2.11}$$

The last two terms in this equation account for nutrient absorption by the healthy and cancer cells, respectively. Both populations compete to feed on the available free nutrient. The rates $\tilde{\gamma}_k(\vec{i})$ depend, of course, on $p_k(\vec{i})$, as indicated in Eq. (2.3).

(v) Bound nutrient concentration. The bound nutrient concentration is given by

$$q_k(\vec{i},t+\tau)=q_k(\vec{i},t)+\tau\times\Bigg[\tilde{\gamma}_k(\vec{i})c(\vec{i})-\tilde{\beta}_k c(\vec{i})+h(\vec{i})\times\sum_{\vec{i}'}^{\mathrm{NN}}\tilde{\alpha}_1(\vec{i}')q_k(\vec{i}')-\tilde{\alpha}_1(\vec{i})q_k(\vec{i})\sum_{\vec{i}'}^{\mathrm{NN}}h(\vec{i}')\Bigg], \tag{2.12}$$

where the term proportional to $\tilde{\beta}_k$ represents the bound nutrient that is being consumed by the cancer cells and the last two terms stand for the nutrient that is transported along by the migrating cancer cells.

Some numerical solutions for this system of coupled nonlinear equations are presented in the next section. Aside from the explicit solutions, it may be useful to find the times at which crucial events, such as the death of an organ or the onset of metastasis, occur. This has to be specifically defined for the particular organ and cancer type under consideration. In relation to organ death, it may be meaningful to find the time at which a given portion $K$ of the cells becomes either cancerous or dead (event $A$). For the case of metastasis we find instead the time at which a proportion $H$ of cells has migrated into the blood vessel (event $B$). Only cancer cells are allowed to enter the blood vessel and the migration of a few cancer cells into it does not necessarily mean metastasis, since the survival probability for cancer cells in the bloodstream is very low [18]. We use absorbing boundary conditions for the cancer cells entering the vessel: any cancer cell arriving at the vessel wall is instantly incorporated into the bloodstream. It may sometimes be necessary to consider that the vessel wall forms a barrier against cell invasion. The inclusion of this barrier in our model and the analysis of its effects, which could have some bearing on event $B$, would be relatively simple. However, since this is not the main point of our paper and we do not want to introduce too many parameters in this presentation of our model, we have omitted a discussion of this problem here.

## III. RESULTS AND DISCUSSION

One of the most striking properties of cancer cells is their ability to proliferate, following a huge range of multiplication rates and generating a wide variety of shapes. This is true even for small variations in the environmental conditions. However, clinical data point to some common features

TABLE I. List of the parameters used for the various cases (Figs. 1–8).

| Figure | $\alpha$ | $\gamma$ | $\tilde{\alpha}$ | $\tilde{\beta}$ | $\tilde{\gamma}$ | $P_0$ | $Q_M$ | $Q_D$ | $P_D$ |
|---|---|---|---|---|---|---|---|---|---|
| 1 | 0.25 | 0.0002 | 0.1 | 0.08 | 0.12 | 1 | 0.5 | 0.12 | 0.2 |
| 2 | 0.25 | 0.0002 | 0.004 | 0.08 | 0.12 | 1 | 0.5 | 0.12 | 0.2 |
| 3 | 0.25 | 0.0002 | 0.02 | 0.07 | 0.1 | | 0.45 | 0.12 | 0.3 |
| 4 | 0.25 | 0.0002 | 0.01 | 0.08 | | 1.3 | 0.4 | 0.12 | 0.2 |
| 5 | 0.25 | 0.0002 | 0.025 | 0.07 | | | 0.5 | 0.12 | 0.25 |
| 6 | 0.25 | 0.0002 | 0.025 | 0.07 | | | 0.5 | 0.12 | 0.25 |
| 7 | 0.25 | 0.0002 | | 0.09 | 0.15 | | 0.5 | 0.12 | 0.25 |
| 8 | 0.25 | 0.0002 | 0.01 | 0.08 | 0.1 | 1.5 | 0.4 | | 0.2 |

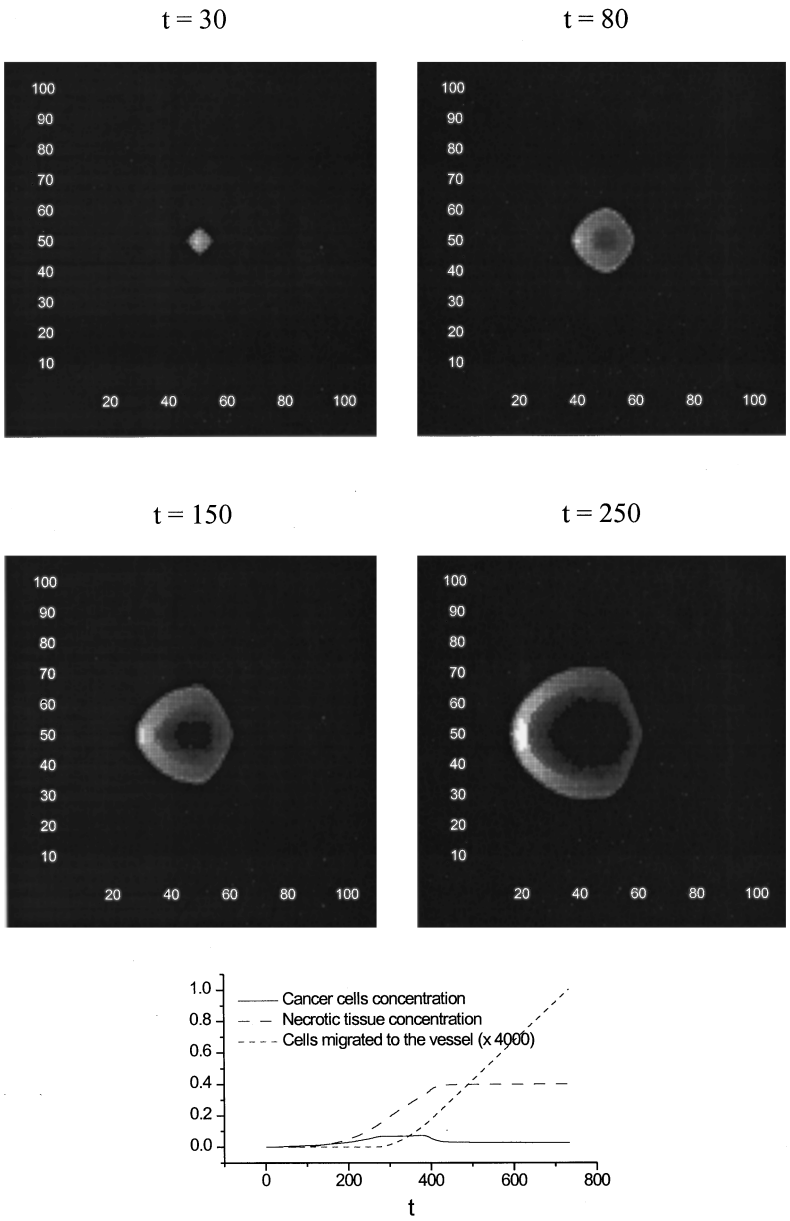


FIG. 1. Snapshots of the growing tumor, at different times. Lightest tones represent the most active regions (highest cancer cell concentrations). The dark region at the center represents the necrotic core. Due to the high cancer cell mobility ($\tilde{\alpha}=0.1$) the growth is almost isotropic.

(e.g., the eventual catastrophic growth of neoplastic tissue) in the evolution of tumor structures [19]. Moreover, as is often the case in biological systems, a chaotic behavior seems to be the general rule. The analysis of the effects of variations of the relevant parameters is the first step to test the validity of the model, which must be capable of predicting a large variability in the growth rates and morphology without destroying those features that are common to cancer growth. Changes in some properties that characterize the cancer type (e.g., the thresholds for multiplication, death, and diffusion) are of course determinant. However, we also expect tumoral behavior to be strongly dependent on the environmental conditions. In this section we try to determine how changes in the environment influence the evolution of the system.

To simplify the presentation of the results, we assume that there is a single relevant nutrient, which, for the reasons expounded in the Introduction, we take to be iron. Since we consider a single nutrient, we omit all subscripts in the following. After an extensive study we find that the iron affinity ($\tilde{\gamma}$) and the diffusion coefficient ($\tilde{\alpha}$) of the cancer cells, and the iron supply (which we assume to be given by the iron concentration $P_0$ at the location of a blood vessel) are the most critical parameters for the characterization of tumoral evolution. Next we use different representations to present a few of the most significant results obtained in our analysis. The parameters chosen for the simulations are reported in Table I for all figures.

We assume that at $t=0$ the nutrient distribution has reached a steady state consistent with the boundary conditions. At that instant, a cancer seed is introduced at the node $\vec{I}$, located at the center of the sample. No dead cells are present as yet. Therefore the initial conditions for our problem are

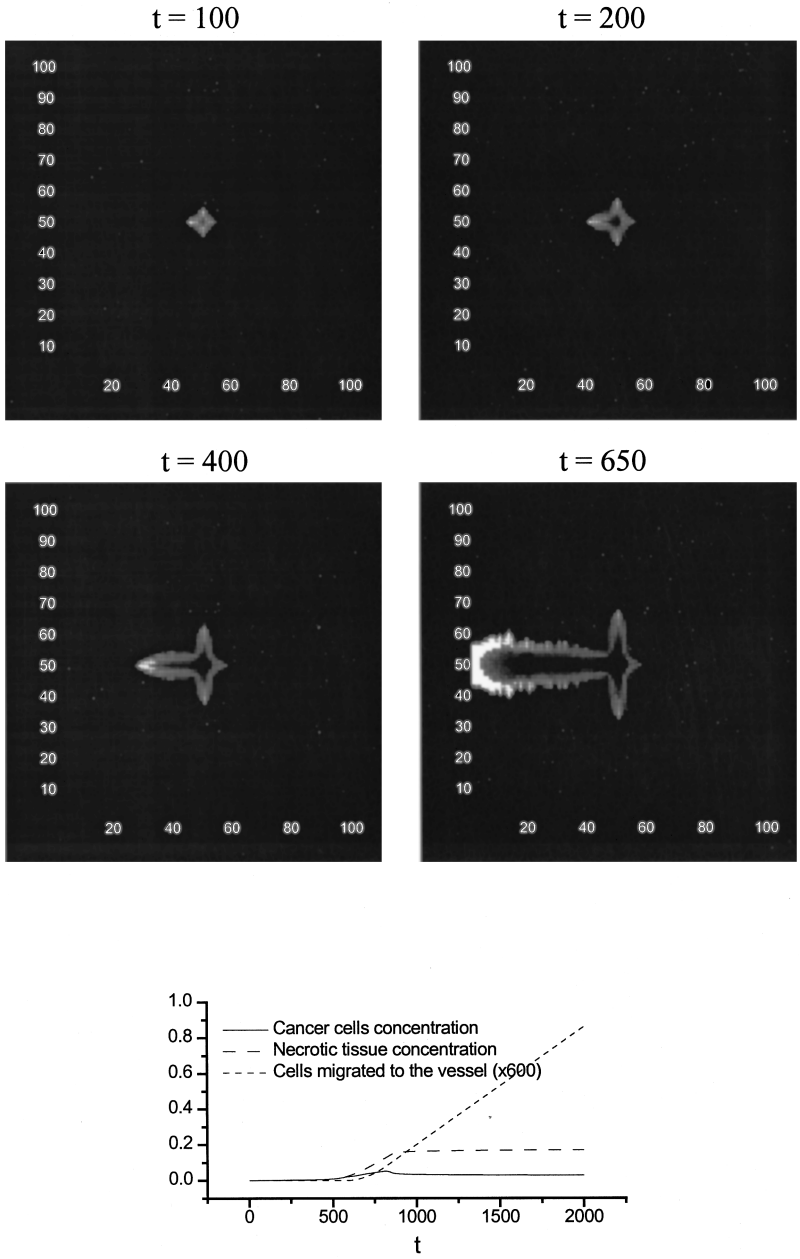


FIG. 2. As in Fig. 1, except that here $\tilde{\alpha}=0.004$ leads to a strongly anisotropic growth.

$$c(\vec{i},0)=c_0\delta(\vec{i}-\vec{I}), \tag{3.1}$$

$$d(\vec{i},0)=0, \tag{3.2}$$

$$q(\vec{i},0)=q_0\delta(\vec{i}-\vec{I}), \tag{3.3}$$

where $c_0$ and $q_0$ represent the initial number of cancerous seed cells and the corresponding amount of bound nutrient, respectively. The free nutrient concentration $p(\vec{i},0)$ is taken to be that corresponding to the steady state of the healthy tissue. The initial amount of bound nutrient per cell, $q_0/c_0$, is assumed to satisfy $Q_D<(q_0/c_0)<Q_M$. We also assume that the total cell population at each node is normalized, so that we take $n=1$.

The sample we consider is a two-dimensional slab of tissue. The nutrient source is a vessel that runs along its left side. The iron concentration there is assumed to remain constant, $p(t)=P_0$. Periodic boundary conditions are used for all quantities at the upper and lower boundaries. To determine $p(\vec{i},0)$ we find a stationary solution of the continuum equivalent of Eq. (1),

$$\dot{p}(x,t)=\alpha\frac{\partial^2 p(x,t)}{\partial x^2}-\gamma p(x,t), \tag{3.4}$$

where we have set $S(t)=0$ and taken advantage of the transverse symmetry of the problem. It can be easily seen that the solution is $p(x)=p_0\exp(-Dx)$, where $D=\sqrt{\gamma/\alpha}$. Once discretized, the solution has the form $p(i)=P_0\exp(-iD)$, where $i=0,\ldots,2I+1$ runs along the lattice nodes.

Time discretization allows us to solve the model equations by successive iterations. The lattice size used in the

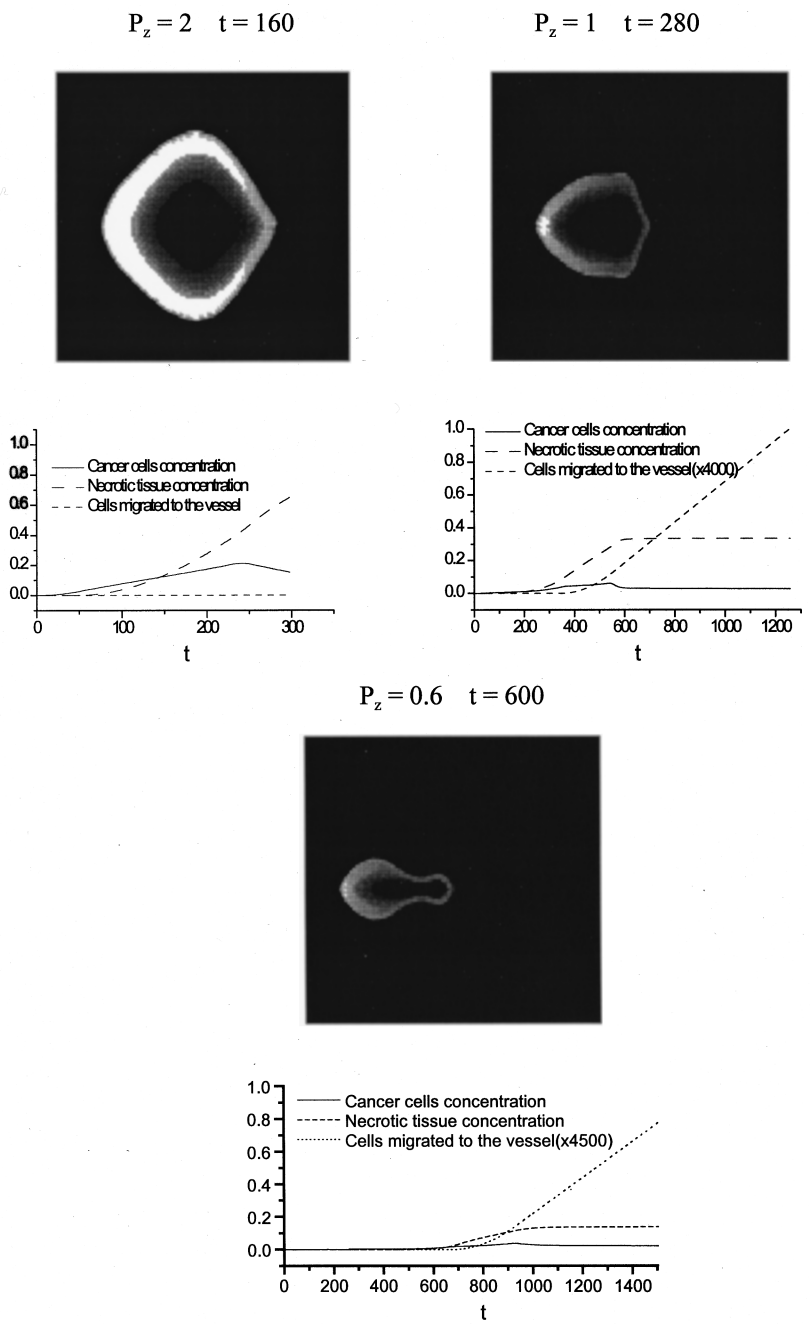


FIG. 3. Snapshots of a growing tumor for various values of the iron concentration at the blood vessel location. Since for brevity only the maps at a single time (which is different for each plot) are reported, the complete time history of the relevant parameter is shown in the linear plots below the maps.

simulations is $100\times100$. For a more realistic study involving a specific tumor pathology, a much finer grid with a relatively short time step would be required. Even in this situation and in the case of three-dimensional (3D) simulations, computer times and costs are quite affordable, especially if parallel processing is adopted [20]. In Figs. 1–4 we show snapshots of the concentration of active cancer cells, the necrotic core usually being represented by a dark region surrounded by cancer cells. Higher concentrations of active cancer cells are depicted in lighter gray tones. The linear plots represent the time evolution of the average concentrations of cancerous and dead cells and of the total number of cancer cells that have migrated into the blood vessel. In all figures, the tumor seed is initially placed at the center of the specimen with a concentration $c_0=0.2$. The nutrient source (the ''vessel'') located at the left edge of the specimen is also a sink for the cancer cells. Figures 1–4 clearly show that variations of a few biochemically relevant parameters within reasonable bounds lead to a wealth of possibilities for neoplastic development.

Comparing Figs. 1 and 2, we observe how the tumor shape is affected by the cancer cell diffusivity $\tilde{\alpha}$. When the tissue is very soft, i.e., when $\tilde{\alpha}$ is high, the tumor grows easily in all directions and the shape remains almost spherical. This can be seen in Fig. 1, where $\tilde{\alpha}=0.1$. The tumor center of mass moves very fast towards the vessel and the

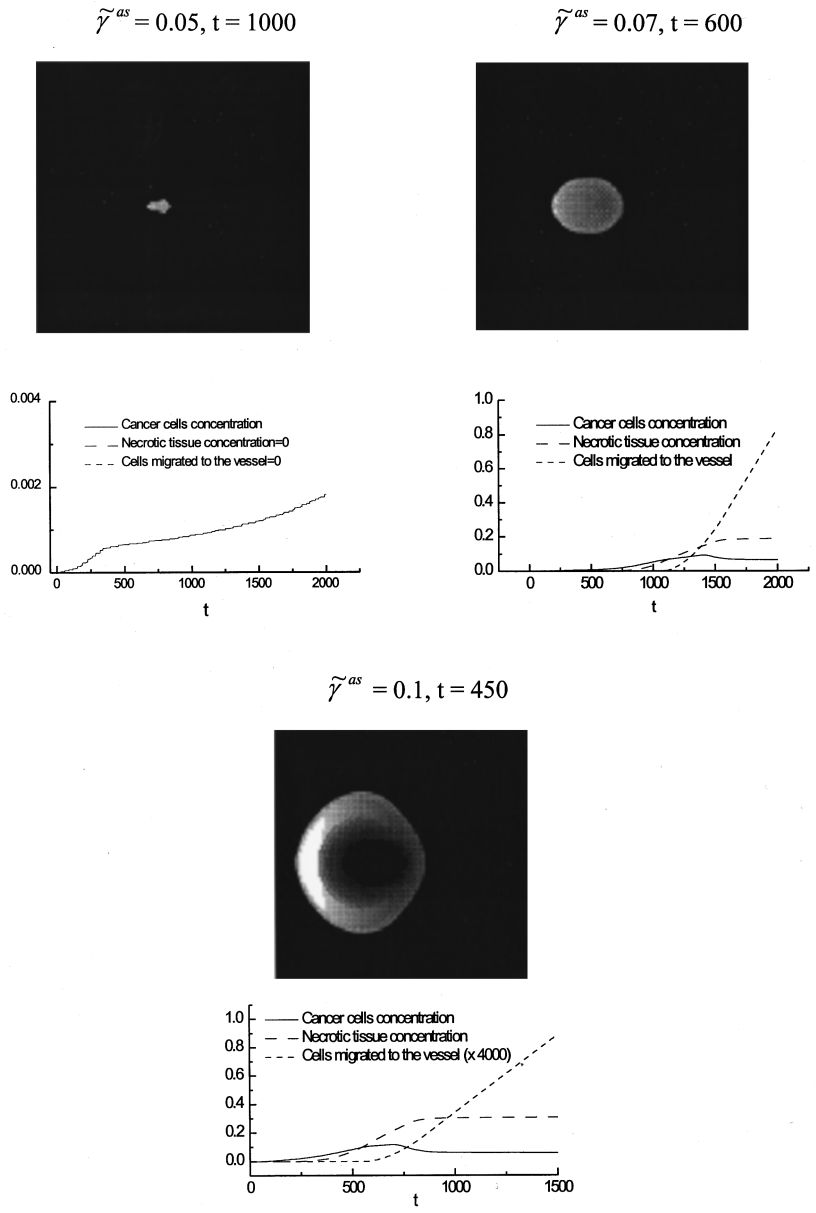


FIG. 4. Snapshots of a growing tumor for various values of the iron binding rate. Since for brevity only the maps at a single time (which is different for each plot) are reported, the complete time history of the relevant parameter is shown in the linear plots below the maps.

necrotic region grows rapidly. From the linear plot, we see that a large amount of dead cells is already present in the tissue when the cancer cells start migrating into the blood vessel. The large growth attained by the tumor at that time means that the survival chances of the tissue are probably very low. Consequently, the arrival at a metastatic stage is unlikely.

A very different situation arises when $\tilde{\alpha}$ is small: see Fig. 2, for which $\tilde{\alpha}=0.004$. The tumor grows rather slowly, developing a highly anisotropic shape. Only those cancer cells migrating towards the vessel find good conditions for reproduction. They also shield from the iron flow the few cancer cells that moved in other directions. In addition to the high activity at the front tip, revealed by the lighter tones, it is interesting to note the jagged tumor edges, quite different from the smooth surface exhibited when $\tilde{\alpha}$ is high (see Fig. 1). The strong directionality in the tumor development leads to a very high probability of metastasis, since only a very small portion of the tissue has become cancerous by the time cancer cells begin migrating into the vessel. These conditions may lead to the formation, starting from a single initial core, of several tumor seeds, with the one closest to the vessel always the most active.

Strong variations in the tumor shape have also been obtained by changing other parameters. Snapshots for different values of the iron availability, characterized by $P_0$, and of the cancer cell iron binding rate $\tilde{\gamma}^{as}$, are reported in Figs. 3 and 4, respectively. Due to the different proliferation rates, the snapshots shown in the various plots refer to different times. In Fig. 3 we observe that the tumor cross-sectional area (as seen from the vessel) decreases with a reduction in the iron supply. Cancer cells respond to a supply reduction with a stronger jump directionality; activity becomes largely confined to the front tumor end.

Figure 4 shows that cancer growth is very sensitive to siderophore efficiency. Indeed, cancer growth demands a

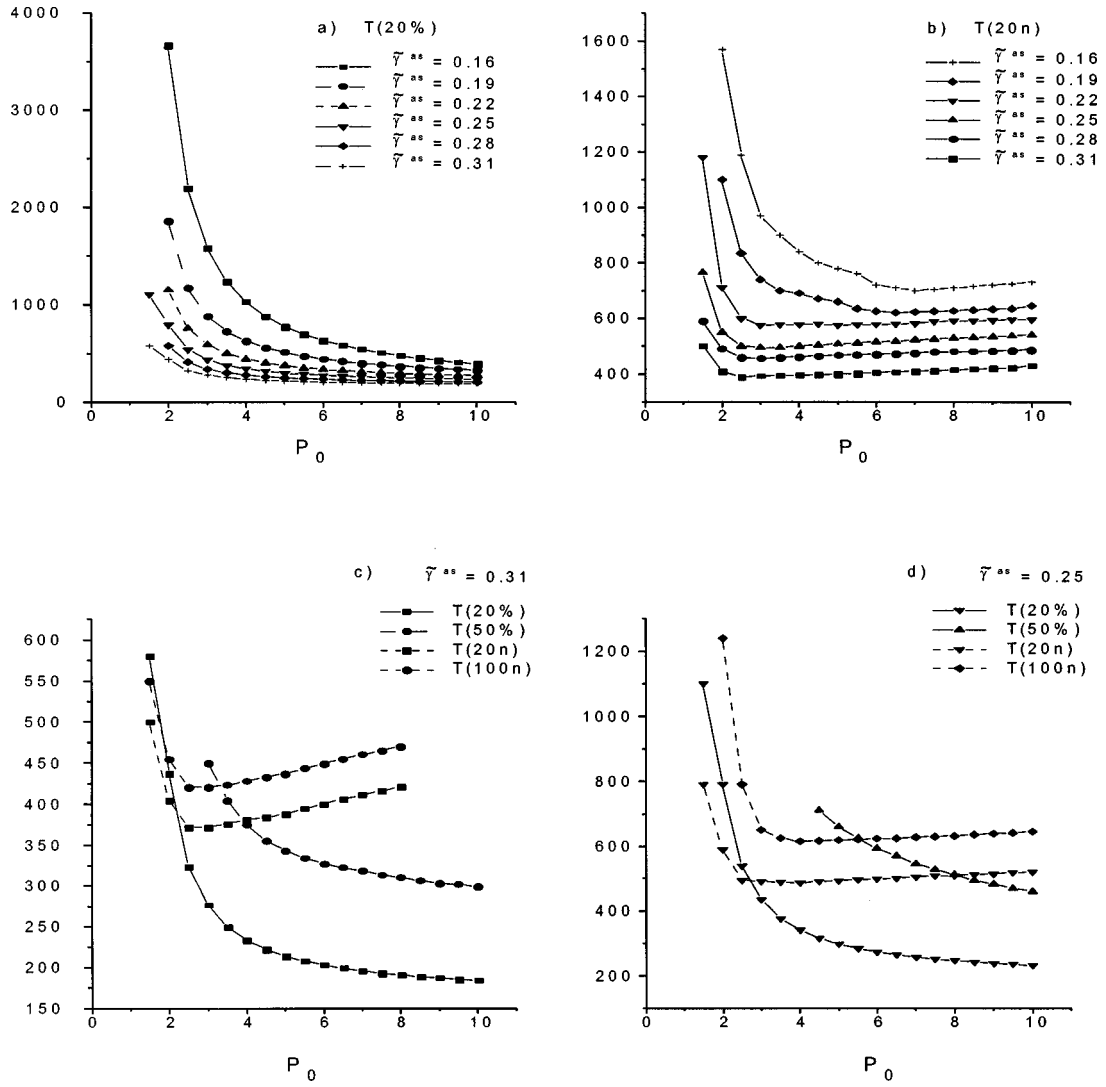


FIG. 5. Comparison of the times $T(K\%)$ for events $A$ and $T(Hn)$ for events $B$ as functions of $P_0$ for several values of $\tilde{\gamma}^{as}$, $K$, and $H$. In events $A$ a portion $K\%$ of the cells becomes cancerous or dead. In events $B$ a portion $H$ of cells has migrated into the blood vessel.

relatively high iron binding rate. If iron uptake is insufficient, the mitosis threshold is seldom reached and the tumor remains latent.

As the linear plots show in all cases considered, once cancerous cells start arriving at the vessel, their migration rate reaches a steady state, leading to a linear growth of the total amount that has entered the bloodstream, while the total number of dead cells levels off. The number of cancer cells remaining in the tissue, on the other hand, reaches a maximum and then starts to decrease once migration into the vessel has begun.

Figures 5–7 report the times required for events $A$ or $B$ (defined in the last paragraph of the preceding section) as functions of the model parameters $P_0$ (Fig. 5), $\tilde{\gamma}^{as}$ (Fig. 6), and $\tilde{\alpha}$ (Fig. 7). More specifically, we call $T(K\%)$ the time needed for a portion $K\%$ of the cells to become either cancerous or dead (event $A$) and $T(Hn)$ the time at which a number $H$ of ''normalization units'' $n$ [as defined in Eq. (2)] of cancerous cells has reached the blood vessel (event $B$).

Figures 5(a) and 5(b) show, for $K=H=20$, that both $T(K\%)$ and $T(Hn)$ decrease with the iron concentration in the vessel $P_0$. For large values of $P_0$, the curves approach an asymptotic value, which can be evaluated analytically. Likewise, for any given $P_0$, an increase in the iron affinity of cancer cells implies a reduction in the event time, i.e., a higher proliferacy rate for the tumor.

The regularity of the curves in this figure suggests a fitting of the form

$$T(K\%)=\theta+\kappa\exp[1/(P_0-\zeta)], \tag{3.5}$$

where $\theta$, $\kappa$, and $\zeta$ are parameters which depend on $\tilde{\gamma}^{as}$ and $K$. The fitting is excellent not only for the reported plots but also for many others (not reported here for brevity). A similar fitting is not possible for the curves of Fig. 5(b), which exhibit a more complex behavior. In fact, for large values of $P_0$, cancerous cells do not significantly diffuse, due to the high iron concentration in the neighborhood. As a consequence, migration is inhibited and the time required by the cancer cells to get into the bloodstream is increased.

In Figs. 5(c) and 5(d) the times for events $A$ and $B$ are plotted as functions of $P_0$ for various values of $\tilde{\gamma}^{as}$, $K$, and $H$. It is interesting to notice that the curves for $T(K\%)$ are above those for $T(Hn)$ for low values of $P_0$ and, vice versa,

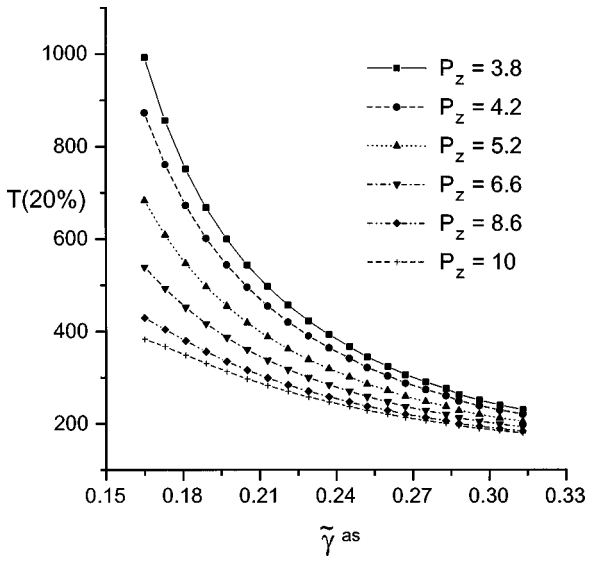


FIG. 6. Time of occurrence of event $A$ as a function of $\tilde{\gamma}^{as}$ for various values of $P_0$. Solid lines correspond to a fitting with Eq. (3.6).

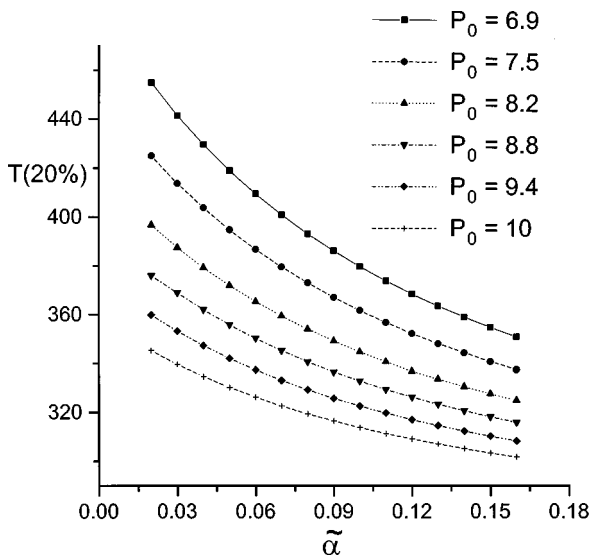


FIG. 7. Time of occurrence of event $A$ as a function of the cancer cell diffusion rate $\tilde{\alpha}$ for various values of $P_0$.

they are below for high values of $P_0$. The intersection points separate regions of high likelihood of patient death, due to the growing cancer, from regions of more likely occurrence of metastasis. The values of $K$ and $H$ that are relevant for a meaningful comparison depend, of course, on the specific details of the developing neoplasia.

In Fig. 6 we report the time $T(20\%)$ of occurrence of event $A$ as a function of the nutrient binding rate $\tilde{\gamma}^{as}$ for several values of $P_0$. We observe that, when the iron affinity is large, the system behavior is weakly sensitive to the iron concentration, which becomes a critical parameter for low iron affinity, as should be expected. Conversely, we see that the curve is rather flat for $P_0=10$, while there is a strong dependence on $\tilde{\gamma}^{as}$ when the iron availability is low ($P_0=3.76$). The family of curves of Fig. 6 again shows an interesting regularity that suggests a fitting with a hyperbolic function,

$$T(K\%)=\theta'+\frac{\kappa'}{(\tilde{\gamma}^{as}-\tilde{\gamma}_c^{as})^{\lambda}}, \tag{3.6}$$

where $\theta'$, $\kappa'$, $\tilde{\gamma}_c^{as}$, and $\lambda$ are parameters that depend on $P_0$ and $K$. In particular $\theta'$ represents the asymptotic value of $T(K\%)$ for a very large $\tilde{\gamma}^{as}$, while $\tilde{\gamma}_c^{as}$ is a critical value of $\tilde{\gamma}^{as}$. When this critical value is reached there is a transition between the death of the patient and the latency of the tumor. In fact, for $\tilde{\gamma}^{as}=\tilde{\gamma}_c^{as}$, $T(K\%)\to\infty$.

A simple argument may be used for an analytical evaluation of $\tilde{\gamma}_c^{as}$. Let us assume that the tumor has reached a stage at the edge between latency and death. Under these equilibrium conditions, the amounts of absorbed and consumed iron must be approximately equal. Likewise, diffusion becomes negligible. Then, from Eq. (2.12) it follows that

$$\tilde{\gamma}_k(\vec{i})=\tilde{\beta}_k(\vec{i}), \tag{3.7}$$

which yields an estimate of $\tilde{\gamma}_c^{as}$ in excellent agreement with the value obtained numerically.

The dependence of the time of occurrence $T(20\%)$ of event $A$ on the diffusion coefficient $\tilde{\alpha}$ is reported in Fig. 7 for several values of $P_0$. For low values of $\tilde{\alpha}$ the cancer growth is strongly determined by the nutrient availability in the blood vessel. On the contrary, when cancer cells can diffuse easily, cancer growth is mostly dependent on the ability of the cells to move to regions where the lack of competition allows them to find high concentrations of free iron. Of course, for high values of $\tilde{\alpha}$, since the availability of bound iron for cancer cells that do not belong to the tumor periphery will rapidly decrease, the necrotic core will also grow very fast.

A different representation is used in Fig. 8, where we plot the temporal evolution of the concentrations of active and necrotic cancer cells and of the number of cells that have migrated into the vessel for several values of the cancer cell death threshold $Q_D$. We distinguish in the plots between an initial stage, when the cancer starts growing, and a ''mature'' stage, when the cancer is already well developed. In the initial stage, as can be more clearly seen from the inset, there is at first a fast growth region, followed by a plateau. This plateau is due to the onset of competition among the cancerous cells, which no longer have access to an unrestricted flow of nutrient. The irregular, almost chaotic behavior of the growth in this initial stage is also remarkable. The fluctuations and the plateau are evident for large values of the death threshold and disappear for lower values. The ''mature'' stage displays three well-defined regions (which can be piecewise approximated by exponentials). In the first of these regions, cancer cell diffusion and reproduction are the dominant phenomena and the total number of cancer cells grows rapidly. The curve has a sudden change in slope when cancer cells start migrating into the vessel: this change of slope corresponds to the first nonzero values in plot (c). The maximum in the cancer cell concentration is reached when the whole region next to the vessel is invaded by the tumor. Starting from this point, the number of cancer cells that have migrated into the bloodstream increases linearly. Finally, the system reaches a steady state: all active cells are provided with enough iron, so that the growth of the necrotic core

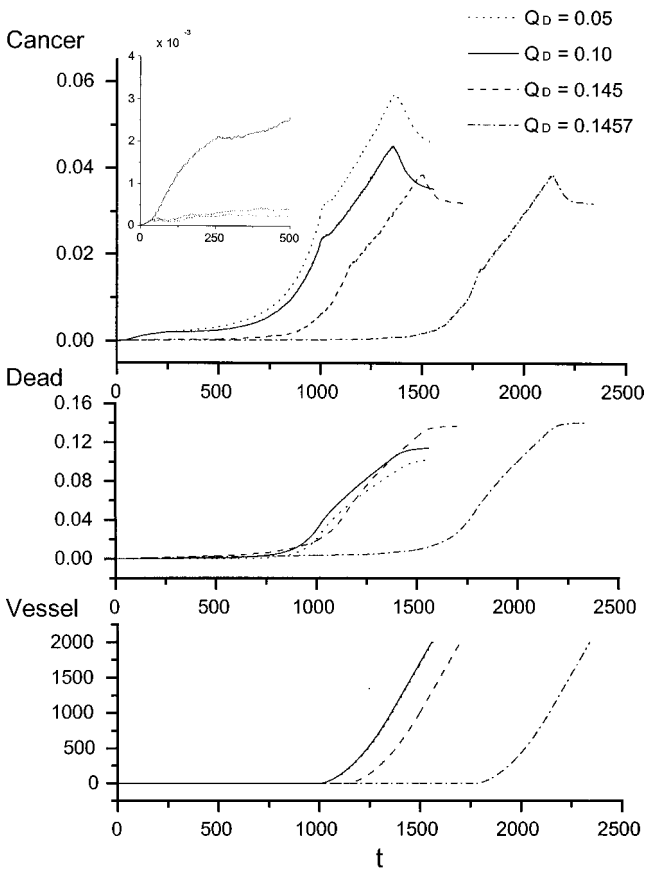


FIG. 8. Time dependence of (a) cancer cell concentration, (b) necrotic cell concentration, and (c) number of cells that migrated into the bloodstream for various values of the death threshold $Q_D$.

stops as shown in plot (b), while newly generated cancer cells correspond to an additional influx into the bloodstream.

Another interesting feature of Fig. 8 is the presence of some accumulation points for the curves, which tend to converge to limit functions in the three plots. This is particularly evident in (c), where the two curves for the lowest values of $Q_D$ are superimposed. Note also how the positions of the ''breaking points'' in (a) collapse to the same time when $Q_D$ decreases.

Latency is observed to occur for high values of the threshold: note the large shift towards long times at the onset of growth in all curves when $Q_D = 0.1457$ (the plateau becomes extremely long). In this case, an interesting effect can be observed: the structure of the neoplastic tissue remains almost constant for a very long time, after which a catastrophic event occurs, leading to a fast growth of the tumor.

## IV. CONCLUSIONS

Using a set of rules formulated on the basis of what is known about tumoral growth, we have developed a consistent mathematical model for this process. Extensive numerical simulations prove that the system described by our model is extremely sensitive to small variations in the values of a few relevant parameters. The solutions confirm that the process of cancer growth is strongly related to the environmental conditions and, in particular, to the availability of basic nutrients. Accordingly, a manifold of different morphologies, growth rates, and outcomes (death, metastasis, or latency) can emerge. Although we have considered iron as the limiting nutrient, other nutrients can also be included in the model.

In the present contribution we have dealt only with tumor evolution in homogeneous media without specific anatomic constraints. Such homogeneous media can be taken to represent soft tissues, such as those in the brain. The morphological correspondence of the result of our simulations with real brain tumors is quite good [21].

We are presently working in several directions to extend and apply our model.

(1) Since immune system cells can develop a high affinity for nutrients, we will include the influence of leukocytes. They are an additional cell population that competes for the available resources.

(2) Anatomical constraints such as bone or cartilage can be easily incorporated, due to the local nature of our model.

(3) Our model already contains stochastic elements: more direct stochasticity can be introduced to simulate tissue inhomogeneities. For example, cancer cell diffusion into soft tissue regions can be modeled by randomly permitting the cancer cells to jump to more distant lattice sites. Figures 1 and 2 suggest that the random introduction of softer regions (higher $\alpha$'s) in an otherwise hard tissue will favor spiderlike morphologies.

(4) We are refining the criteria for quantitatively determining tumor aggressiveness and its relation to tumor morphology, tissue or organ death, and the likelihood of metastasis.

(5) A very important addition will be the explicit inclusion of vascularization. In fact, from our discussion it follows that cancer cells are likely to emit an angiogenic signal once their iron content ($q_{ij}$) falls below a certain threshold $Q_A > Q_D$. Thus we will need to introduce in our equations a coupling between the variables $q_{ij}$ and the nutrient sources [22].

(6) Rapidly reproducing organisms are especially sensitive to short-wavelength radiation. This is the reason why some cancers are successfully treated using radiation. The model is ideally suited for incorporating at any given stage (fixed $t$) any chosen flow of radiation (of specified frequency and kind) or chemotherapeutical agents. Thus, once it has been sufficiently refined with the addition of all necessary ingredients to make it realistic and reliable, it can be used for suggesting an optimization of therapy.

## ACKNOWLEDGMENTS

This research was partially supported by the Ministero dell'Universitá della Ricerca Scientifica e Tecnologica (Italy) and by the National Science Foundation through Grant No. HRD-9450342.

[1] *A Survey of Models for Tumor-Immune System Dynamics*, edited by J. A. Adam and N. Bellomo (Birkhäuser, Boston, 1997).
[2] A. C. Burton, Growth **30**, 159 (1966).
[3] L. Glass, J. Dyn. Syst. Meas. Control **95**, 324 (1973).
[4] R. M. Shymko and L. Glass, J. Theor. Biol. **63**, 355 (1976).
[5] H. P. Greenspan, J. Theor. Biol. **56**, 229 (1976).
[6] M. A. J. Chaplain, D. L. Benson, and P. K. Maini, Math. Biosci. **121**, 1 (1994).
[7] See Ref. [1], p. 187.
[8] C. J. Eskey, A. P. Koretsky, M. M. Domach, and R. K. Jain, Proc. Natl. Acad. Sci. USA **90**, 2646 (1993).
[9] H. H. Sussman, in *Iron and Tumor Cell Growth, Iron in Immunity, Cancer and Inflammation*, edited by M. de Sousa and J. H. Brock (Wiley, New York, 1989).
[10] M. Cazzola, G. Bergamaschi, L. Dezza, and P. Arosio, Blood **75**, 1903 (1990).
[11] M. de Sousa, Pathol. Res. Pract. **190**, 840 (1994); R. Gopalakrishna, Z. H. Chen, and U. Gundimeda, Proc. Natl. Acad. Sci. USA **91**, 12 233 (1994).
[12] T. Inoue, P. G. Cavanaugh, P. A. Steck, N. Brunner, and G. L. Nicolson, J. Cell Physiol. **156**, 212 (1993).
[13] E. H. Morgan, in *Comparative Iron Metabolism, Iron in Biochemistry and Medicine*, edited by A. Jacobs and M. Worwood (Academy, London, 1980), Vol. II.
[14] Th. Höfer, J. A. Sherratt, and P. K. Maini, Physica D **85**, 425 (1995).
[15] J. C. M. Mombach and J. Glazier, Phys. Rev. Lett. **76**, 3032 (1996).
[16] F. Schweitzer, W. Ebeling, and B. Tilch, Phys. Rev. Lett. **80**, 5044 (1998).
[17] R. Halvorsrud and G. Wagner, Phys. Rev. E **57**, 941 (1998).
[18] E. Ruoslahti, Sci. Am. (Int. Ed.) **275**, 72 (1996).
[19] J. W. Uhr, R. H. Sheuermann, N. E. Street, and E. S. Vitetta, Nat. Med. (N.Y.) **3**, 505 (1997).
[20] P. P. Delsanto, R. S. Schechter, H. H. Chaskelis, and R. B. Mignogna, Science **295**, 1188 (1994); P. P. Delsanto *et al.*, Wave Motion **20**, 295 (1994).
[21] G. Helmlinger, F. Yuan, M. Dellian, and R. K. Jain, Nat. Med. (N.Y.) **2**, 271 (1997).
[22] Y. Otha, Y. Watanabe, S. Murakami, M. Oda, Y. Hayashi, A. Nonomura, Y. Endo, and T. Sasaki, Br. J. Cancer **76**, 1041 (1997).